CHEMISTRY
A EUROPEAN JOURNAL

DOI: 10.1002/chem.200700334

Solution-Phase Synthesis and High Photocatalytic Activity of Wurtzite ZnSe Ultrathin Nanobelts: A General Route to 1D Semiconductor Nanostructured Materials

Shenglin Xiong, Baojuan Xi, Chengming Wang, Guangcheng Xi, Xiaoyan Liu, and Yitai Qian*[a]

Abstract: A general and facile synthetic route has been developed to prepare 1D semiconductor nanomaterials in a binary solution of distilled water and ethanol amine. The influence of the volume ratio of mixed solvents and reaction temperature on the yield and final morphology of products was investigated. Significantly, this is the first time that wurtzite ZnSe ultrathin nanobelts have been synthesized in solution. It has been confirmed that the photocatalytic activity of ZnSe nanobelts in the photodegradation of the fuchsine acid is higher than that of TiO_2 nanoparticles. The present work shows that the solvothermal route is facile, cheap, and versatile. Thus, it is very easy to realize scaled-up production, and brings new light on the synthesis and self-assembly of functional materials.

Keywords: nanobelts · nanostructures · photocatalysis · semiconductors

Introduction

Environmental problems, such as organic pollutants and toxic water pollutants, provide the impetus for fundamental and applied research into environmental areas. Semiconductor photocatalysis furnishes us with the potential for complete elimination of toxic chemicals, through its efficiency and broad applicability.[1] For commercial applications as a photocatalyst, a material must have superior photocatalytic activity, and also be easily prepared. Over the last few years, considerable efforts have been made in the controlled synthesis of various nanoscaled materials for photocatalysis, to improve their properties. Recently, transition metal sulfides, in particular ZnS and CdS, have been extensively studied, owing to their unique catalytic activity compared to that of TiO_2.[1c,2,3] However, photocatalytic applications of selenide nanostructures have rarely been reported. As an important type II-VI semiconductor, with a room temperature bulk band gap of 2.70 eV (460 nm), ZnSe is a promising functional material for optoelectronic devices, owing to a significantly large exciton binding energy (21 meV)[4] in comparison to GaAs (4.2 meV)[5]. The unique structures, could exhibit new properties and applications in many fields. Therefore, much effort has been devoted to fabricating various ZnSe nanostuctures (such as wires, belts, tubes, and spheres).[6] Although ZnSe nanoribbons have been prepared by means of laser ablation of ZnSe powders at high temperature (950 °C),[6a] to the best of our knowledge, the synthesis of the wurtzite-phase of ZnSe ultrathin nanobelts through a solution-based route at low temperature has not been reported previously.

In this paper, we report a general approach for the preparation of 1D semiconductor nanomaterials in a binary solution, made of distilled water and ethanol amine (EA). More importantly, this is the first time the synthesis of wurtzite ZnSe nanobelts has been achieved in solution. High-magnification transmission electron microscopy (TEM) provides images that show that flexible and ultrathin nanobelts with a thickness of only 5 nm and width of ≈30–80 nm have been produced. It has been confirmed that the photocatalytic activity of ZnSe nanobelts in the photodegradation of the fuchsine acid is higher than that of TiO_2 nanoparticles, which could be assigned to the larger specific surface area of the ZnSe nanobelts (so that they can provide more reactive adsorption/desorption sites for photcatalytic reaction) compared to commercial TiO_2 powders.

[a] Dr. S. Xiong, B. Xi, C. Wang, Dr. G. Xi, Dr. X. Liu, Prof. Y. Qian
Hefei National Laboratory for Physical Sciences at Microscale and the Department of Chemistry
University of Science and Technology of China
Hefei, Anhui, 230026 (China)
Fax: (+86)551-360-7402
E-mail: ytqian@ustc.edu.cn

Results and Discussion

X-ray diffraction (XRD) analysis was used to determine the phase purity of the nanoribbons. As shown in Figure 1, all of the peaks in the XRD pattern can be readily indexed to the

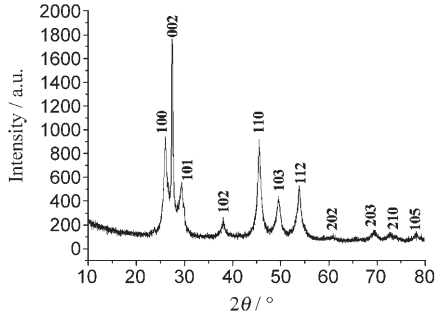

Figure 1. a) XRD pattern of the ZnSe nanoribbons prepared at 220 °C for 24 h.

hexagonal wurtzite ZnSe, with lattice constants of $a = 3.961$ and $c = 6.50$ Å, which agrees with the reported data ($a = 3.997$ and $c = 6.547$ Å, in the JCPDS file, no. 80–008). No other peaks for impurities were detected.

The fine structural details of the as-obtained products were examined by means of the TEM technique. Figure 2a shows a low-magnification TEM image of a ZnSe sample, revealing that the products are composed of a large quantity of beltlike structures that have typical lengths of up to several micrometers. The high-magnification TEM image (Figure 2b) shows a flexible and ultrathin nanobelt with a width

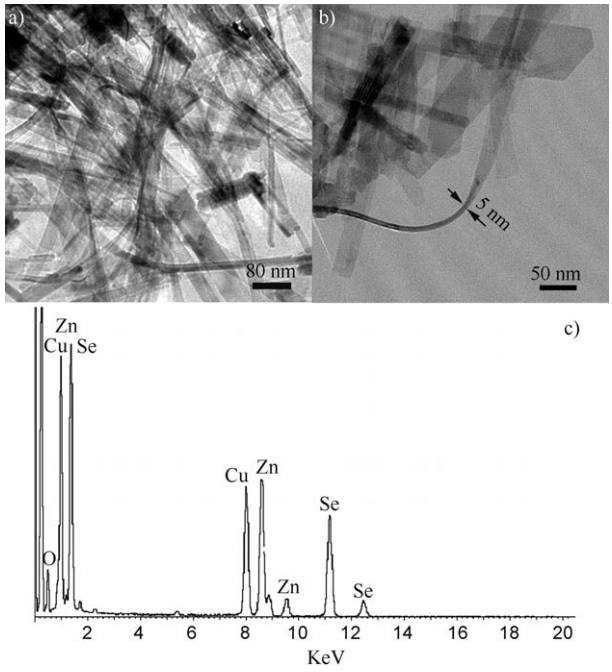

Figure 2. a) A low-magnification TEM image and b) a high-magnification TEM image of a ZnSe sample. c) EDS spectrum taken from a nanobelt.

of ≈30–80 nm and thickness of ≈5 nm. The chemical composition of these nanobelts is further characterized by using energy-dispersive spectroscopy (EDS, Figure 2c). Peaks of the elements Zn and Se are detected in the EDS pattern and the molar ratio is about 1:1 (the O signal derives from the surface absorption of nanobelts and the Cu signal comes from the copper grid).

Significant information about the quality and surface composition of the products can be further provided by using X-ray photoelectron spectroscopy (XPS), as shown in Figure 3. The binding energies obtained in the XPS analysis were corrected for specimen charging, through referencing the C 1s to 284.60 eV. The binding energy of Zn $2p^3$ is identified at 1020.5 eV (Figure 3b), although, Se 3d is found to be 53.86 eV (Figure 3c). The signals at 10.0 and 990.15 eV can be assigned to the binding energy of Zn 3p and the kinetic energy of Zn LMM, respectively. The signal at 401 eV can be attributed to N 1 s, which is derived from ethanol amine absorbed onto the nanoribbons, which is consistent with the results of the FTIR spectroscopy (data not shown). High-resolution XPS for the O 1s region (Figure 3e) indicates that only one oxygen contribution exists here: The core levels centred at about 532 eV can be assigned to the small amounts of physically absorbed H_2O,[7] which further demonstrates the as-obtained products are pure ZnSe.

The typical room-temperature Raman spectrum of ZnSe nanoribbons (Figure 4) shows two bands in the range 150–400 cm^{-1}. The peaks located at around 206, and 252.6 cm^{-1}, these correspond to the transverse optical (TO) and longitudinal optic (LO) phonon modes of ZnSe, respectively. No vibration modes owing to impurities are observed. According to previous results,[8–11] the LO phonon frequency of a single-crystalline ZnSe film is 254 cm^{-1} and that of a single-crystal of ZnSe is 255 cm^{-1} at room temperature. Both indicate a broad Raman peak, owing to the high surface-to-volume ratio of small particles. Compared to the above reports, the TO and LO phonon frequencies of the as-obtained ZnSe sample are both shifted towards a lower frequency, which may be an effect of small size and high surface area of the sample. The relatively sharp and symmetric Raman peaks of the ZnSe nanostructures imply that the ZnSe nanobelts are single crystalline, which is consistent with the following high-resolution TEM (HRTEM) observations.

The microstructural details of nanobelts are further provided by using HRTEM and fast Fourier transformation (FFT) electron diffraction (ED) patterns. Shown in Figure 5a is a TEM image of an individual ZnSe nanoribbon. It can be observed that the nanoribbon is long and straight and has a uniform width along its entire length. Typical widths of the nanoribbon are in the range of 45–50 nm. Figure 5b indicates a typical FFT pattern recorded from this nanoribbon; it can be indexed to the [010] zone axis of the hexagonal ZnSe. These pattern spots confirm the single crystallinity of this ZnSe nanobelt. Shown in Figure 5c is a HRTEM image recorded near the edge of this ZnSe nanoribbon. The regular spacings of the observed lattice planes

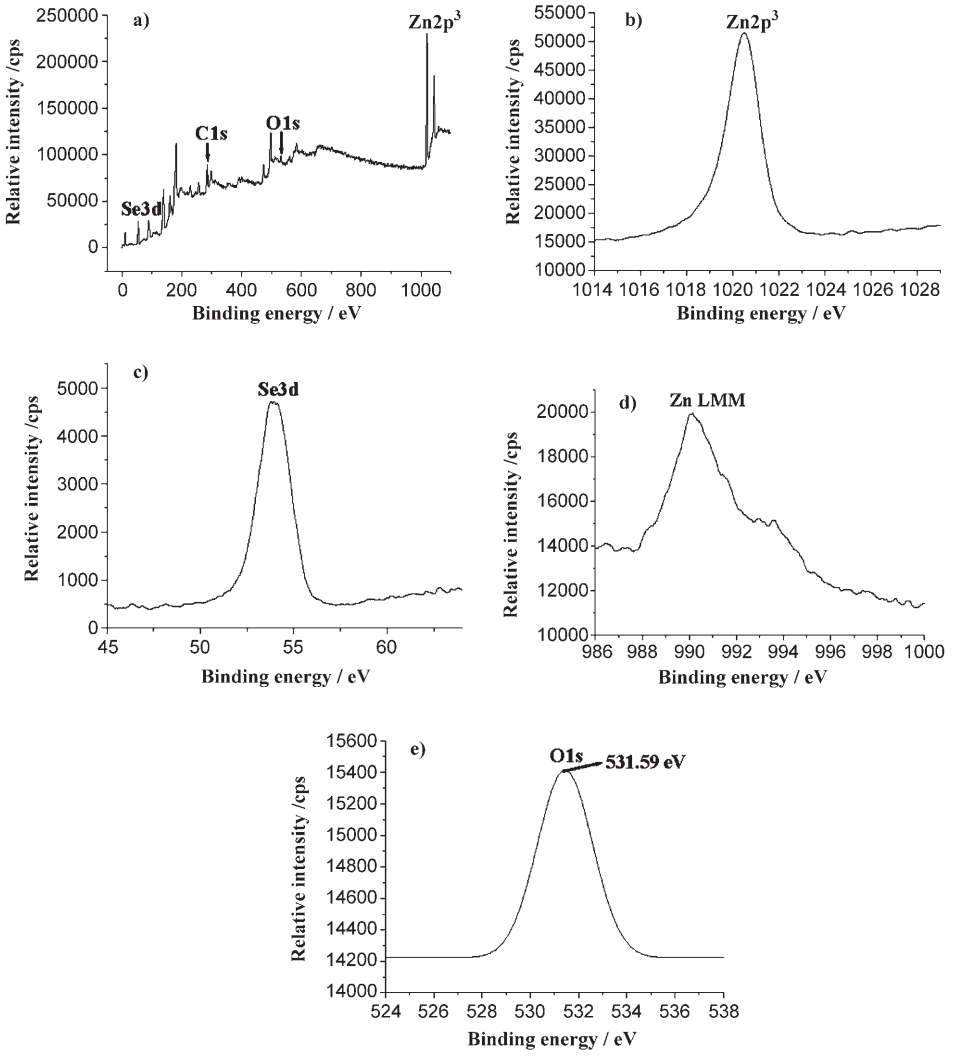

Figure 3. XPS spectra of ZnSe nanoribbons prepared at at 200 °C for 24 h. a) Survey spectrum, b) Zn $2p^3$, c) Se 3d, d) Zn LMM, and e) O 1s.

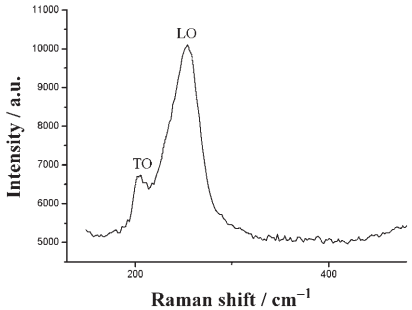

Figure 4. Room-temperature Raman spectrum of ZnSe nanobelts that were produced at 220 °C over 24 h.

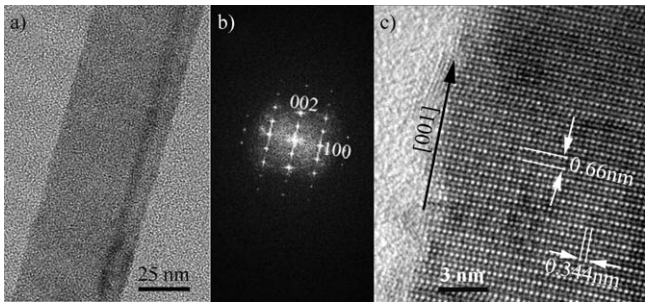

Figure 5. a) A TEM image of a typical nanobelt. b) The corresponding electron diffraction pattern. c) A HRTEM image taken from the side of the nanoribbon.

are ≈0.66 and 0.34 nm, which is consistent with the separation of (001) and (100) planes of hexagonal ZnSe, respectively. It also reveals that the ribbon is single crystalline, structurally uniform, and dislocation-free. Further studies of both the HRTEM image and FFT pattern confirm that the axis growth plane is (001) and the growth direction is preferentially along [001] (*c*-axis).

Further studies show that the water-to-EA ratio plays a significant role in the formation of ribbonlike ZnSe nanocrystals. The formation of flexible nanoribbons is accessible only within a very narrow composition range of the binary solution, this suggests that the ethanol amine plays a crucial role in shaping such flexible and ultrathin ZnSe nanoribbons (Figure 6). If the volume ratio of EA/water is increased to 24:1, beltlike ZnSe nanocrystals are formed accompanied by nanostructures of irregular shapes. However, if the volume ratio of EA/water is decreased to 4:1 or 3:2, the TEM images indicate that the short nanorods (or flakes) and nanoparticles coexist in the products.

It is generally believed that materials that have a hexagonal crystal structure have a particular tendency to grow anisotropically, as the (001) planes indicate different surface energies relative to the (100) and (110) crystal planes.[12] Furthermore, in most reported colloidal synthesis of metal or semiconductor 1D nanocrystals, the anisotropic growth of the 1D structure is often driven by using capping ligands that could bind selectively onto particular facets of the seed particles.[13] Therefore, it is reasonable to

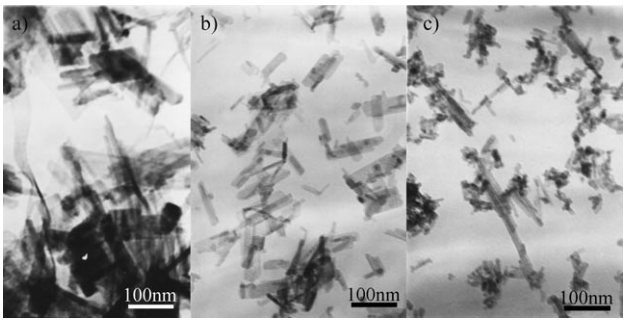

Figure 6. TEM images of ZnSe crystals obtained under different conditions: a) $V_{H_2O}/V_{EA}=1/24$, b) $V_{H_2O}/V_{EA}=1/4$, and c) $V_{H_2O}/V_{EA}=2/3$. The molar ratio $Zn(Ac)_2/Na_2SeO_3=1:1$, for a reaction over 24 h at 220 °C.

conclude that, in our approach, the reagent ethanol amine might adsorb onto the (010) and (100) planes of the incipient ZnSe nuclei, possibly as a result of the match between the special ZnSe atomic surface structures and the linear molecular structure of ethanol amine, and thus making (001) a higher energy face compared to the EA-covered (010) and (100). Direct evidence for this hypothesis requires further study, and the work is under way. The selective absorption of ethanol amine onto some facets, not only prevents the particles from agglomeration, but also influences the growth of the planes, which were strongly in favor of anisotropic growth of new born ZnSe nuclei along [001] axis. This is confirmed by the HRTEM results. In the synthesis of inorganic nanostructures, this may be in accord with the fact that the crystal growth is modulated extrinsically by means of solvent absorption on certain crystallographic facets, which inhibits the growth of some crystal planes, and leads to different growth rates during the growth process of particles, thus generating certain novel crystal shapes.[14] This binary solution reaction system is quite complicated, and the for the formation of certain nanostructures the system needs further modification. Clearly, the synergetic effects of ethanol amine and water could also exert a key influence on the morphology of ZnSe nanostructures. The reaction temperature also plays a key role in the formation of nanoribbons. If the temperature is lower than 180 °C, pure-phase ZnSe can not be obtained. The experimental results reveal that a reaction temperature ranging from 200 to 220 °C is the optimum for the formation of flexible and thin nanoribbons. Further work to better understand the formation of ZnSe nanoribbons is under way.

To demonstrate the potential applicability in photocatalysis of the as-obtained ZnSe nanobelts, we investigated their photocatalytic activity, relative to that of commercial TiO_2 powders. The photocatalytic degradation of fuchsine acid was chosen as a reference and the characteristic absorption of the acid seen at 545 nm was selected for monitoring the adsorption and photocatalytic degradation process. The absorption spectra of an aqueous solution of fuchsine acid (initial concentration: 1.0×10^{-4} M, 20 ml) in the presence of ZnSe nanoparticles (10 mg) under exposure of a UV-light lamp (30 W) for various durations can be seen in Figure 7a.

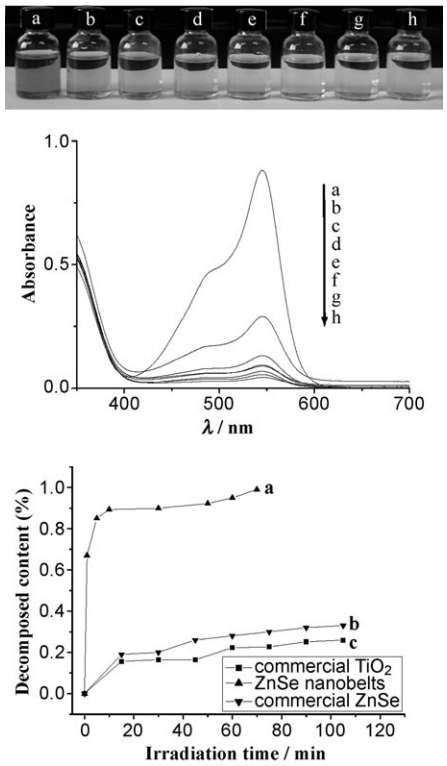

Figure 7. Color change and absorption spectrum of a solution of fuchsine acid (1.0×10^{-4} M, 20 ml) in the presence of ZnSe nanobelts (10 mg) under exposure to UV light: a) initial solution; b–h) solutions with addition of ZnSe nanobelts illuminated for b) 1, c) 5, d) 10, e) 30, f) 50, g) 60, h) 70 min (top and middle). The fraction of the degraded fuchsine acid in the presence of ZnSe nanobelts, commercial ZnSe and commercial TiO_2 powders, respectively, as photocatalysts under exposure to UV light (bottom).

The absorption peak corresponding to fuchsine acid at 545 nm diminishes sharply and even disappears completely after irradiation for about 70 min, compared to the intensity of the initial fuchsine acid solution.

Further experiments were performed to compare the catalytic activity of the ZnSe nanoribbons (10 mg), commercial ZnSe (10 mg) and commercial TiO_2 powders (10 mg) under UV-light exposure. The data of curve a, b and c in Figure 7 (middle) make clear that these ZnSe nanobelts have a higher photodegradation rate than commercial ZnSe, or commercial TiO_2, under the same conditions after exposure to UV light. In Figure 7 curve a, fuchsine acid is degraded by 87.8% on ZnSe nanobelts in only 10 min. In contrast, the degradation rate of commercial ZnSe and TiO_2 is very slow and only 33% (curve b), 25.6% (curve c) of fuchsine acid is decomposed after 105 min, respectively. The higher photocatalytic activity of these ZnSe nanobelts could be assigned to the following two factors. First, ZnSe nanobelts (about $92\ m^2g^{-1}$) have the larger specific surface area compared to commercial TiO_2 powder ($\approx45\ m^2g^{-1}$) and commercial ZnSe. As a result, they can provide more reactive adsorption/desorption sites for photcatalytic reactions. Second, the high crystallinity implies few defects in the as-prepared

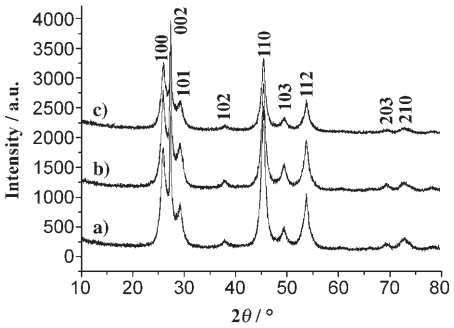

Figure 8. XRD patterns of ZnSe nanobelts; a) before irradiation, b) irradiated for 60 min, and c) irradiated for 100 min by means of UV light.

nanoparticles. It is well known that these defects may serve as recombination centers for photoexcited electron-hole pairs during photocatalysis, this would decrease the photocatalytic activity. A more detailed investigation of photocatalytic activity of ZnSe nanobelts is under way.

The stability of a photocatalyst always influences its application, and doped TiO_2 photocatalysts also endure this problem.[15] Figure 8 reveals the XRD patterns of the as-prepared samples that were subjected to irradiation for different times. The data indicates that the crystal structure of the ZnSe did not change after the photocatalytic reaction, this demonstrates that the ZnSe nanocrystals are stable and do not decompose (or photocorrode) during the photocatalytic process. Although, it is known that bulk ZnSe subjected to irradiation decomposes, particularly in acidic medium, whereas, TiO_2 is stable under irradiation. The stability of ZnSe nanobelts might result from the quantum-size effect. However, the exact nature is not clear and requires further study.

Stimulated by the successful synthesis of ZnSe nanoribbons, we have extended our fabrication to other types of metal chalcogenide nanocrystals. Six other types of metal chalcogenide nanocrystals 1D nanostructures have been successfully synthesized and the results are summarized in Table 1.

The phase and purity of the remaining six types of metal chalcogenide nanocrystals produced by means of the current route were verified by examining their XRD patterns (Figure 9). All the reflection peaks can be indexed to pure wurtzite ZnS (JCPDS Card No. 36–1450), wurtzite CdS

Table 1. Summary of various morphologies of metal chalcogenide nanocrystals fabricated at different experimental conditions.[a]

Sample	Reagents	$V_{H_2O}:V_{EA}$	T [°C]	Morphology
1	1 mmol $Zn(Ac)_2$ +1 mmol Na_2SeO_3	1:9	220	nanobelts
2	1 mmol $Zn(Ac)_2$ +2 mmol L-cysteine	3:2	220	nanorod bundles
3	1 mmol $Cd(Ac)_2$ +1 mmol Na_2SeO_3	1:4	120	nanowire bundles
4	1 mmol $Cd(Ac)_2$ +2 mmol L-cysteine	1:9	180	nanorod bundles
5	1 mmol $Mn(Ac)_2$ +2 mmol L-cysteine	1:9	120	nanowires
6	3 mmol $Pb(Ac)_2$ +1 mmol L-cysteine	2:3	220	nanorods
7	(1 mmol $SbCl_3$ +4 mmol tartrate) +0.5 mmol Na_2SeO_3	1:1	180	nanowires

[a] The reactions are all run for 24 hours.

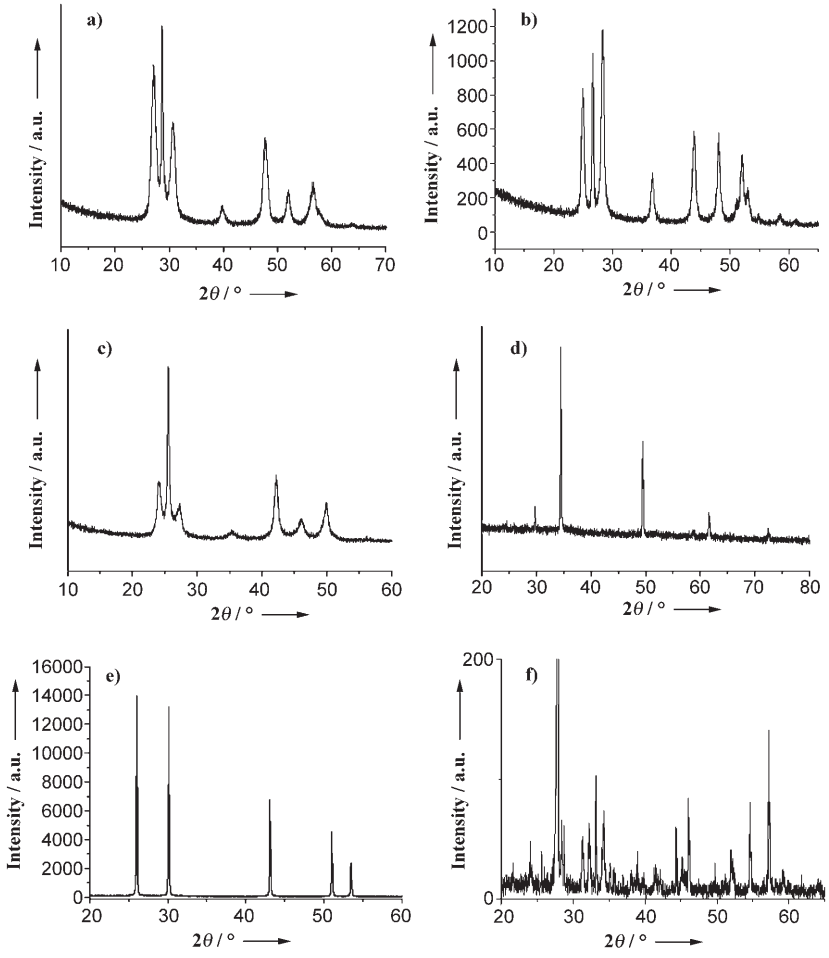

Figure 9. XRD patterns of: a) ZnS nanorod bundles prepared at 220 °C for 24 h, $V_{H_2O}/V_{EA}=3:2$; b) CdS crystals prepared at 180 °C for 24 h, $V_{H_2O}/V_{EA}=1:9$ c) CdSe wires prepared at 120 °C for 24 h, $V_{H_2O}/V_{EA}=1:4$; d) MnS nanowires prepared at 120 °C for 24 h, $V_{H_2O}/V_{EA}=1:9$; e) PbS nanorods prepared at 220 °C for 24 h, $V_{H_2O}/V_{EA}=2:3$; f) Sb_2Se_3 nanowires prepared at 180 °C for 24 h, $V_{H_2O}/V_{EA}=1:1$.

(JCPDS Card No. 41–1049), wurtzite CdSe (JCPDS Card No. 77–2307), alabandite MnS (JCPDS Card No. 06–0518), cubic PbS (JCPDS Card No. 5–0592), and orthorhombic Sb_2Se_3 (JCPDS Card No. 15–861), respectively. No other peaks for impurities were detected.

The panoramic morphologies of the as-obtained ZnS, CdS, CdSe, MnS, PbS, and Sb_2Se_3 were examined by using field emission scanning electron microscopy (FESEM). The diameter of the ZnS nanorods is 13 nm on average and their lengths are in the range of 150–250 nm (Figure 10a). Figure 10b shows a typical FESEM image of CdS fan-shaped nanorod bundles that have a diameter of 14 nm and a length of approximately 300–400 nm. The CdSe samples form bundlelike nanowires that have a diameter of about 20 nm (Figure 10c). The MnS samples form nanowires that have a diameter of around 40–50 nm and a length of up to several micrometers (Figure 10d). The PbS samples contain some microrods that have a diameter of 300–400 nm and a length of several micrometers (Figure 10e). A typical FESEM image of Sb_2Se_3 nanowires that have a diameter of 35 nm and a length up to several tens of micrometers can be seen in Figure 10f. The above results show that the new reaction medium for controlling the morphology of semiconductor nanostructures is effective and general.

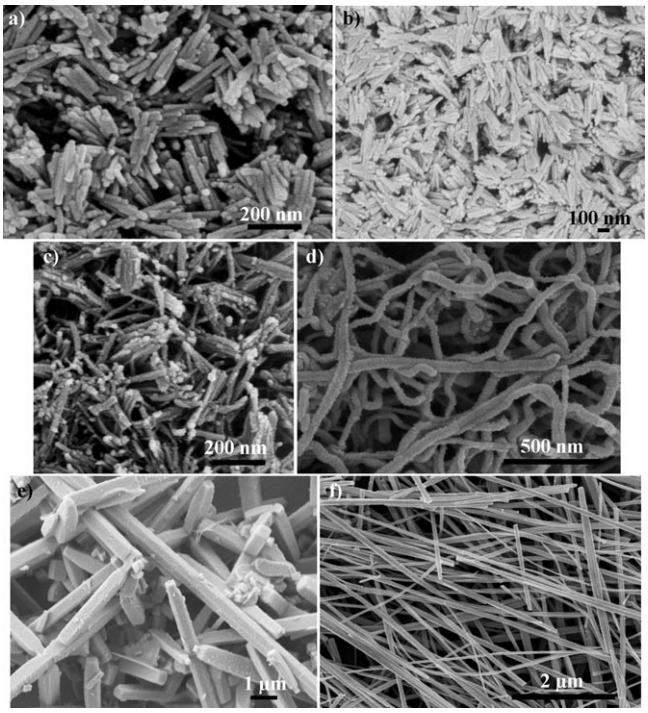

Figure 10. FESEM of: a) ZnS nanorod bundles prepared at 220 °C for 24 h, $V_{H_2O}/V_{EA}=3:2$; b) CdS nanorod bundles prepared at 180 °C for 24 h, $V_{H_2O}/V_{EA}=1/9$; c) CdSe nanowire bundles prepared at 120 °C for 24 h, $V_{H_2O}/V_{EA}=1:4$; d) MnS nanowires prepared at 120 °C for 24 h, $V_{H_2O}/V_{EA}=1:9$; e) PbS nanorods prepared at 220 °C for 24 h, $V_{H_2O}/V_{EA}=2:3$; f) Sb_2Se_3 nanowires prepared at 180 °C for 24 h, $V_{H_2O}/V_{EA}=1:1$.

Conclusion

In conclusion, we have developed a simple and general method to prepare semiconductor 1D nanostructures. To the best of our knowledge, this is the first time that the synthesis of ZnSe nanobelts in solution has been achieved. The effects of the volume ratio of water and ethanol amine, and reaction temperature, on the morphology of ZnSe were investigated. The ultrathin ZnSe nanobelts display higher photocatalytic activity than commercial TiO_2 powders. The high photocatalytic activity of these ZnSe nanobelts is related to the larger surface area and smaller crystal size. The simple process, general strategy, and fine quality of products in this work make the present route both attractive and significant.

Experimental Section

In a typical synthesis, zinc acetate ($Zn(Ac)_2{\cdot}2H_2O$, 1 mmol) and Na_2SeO_3 (1 mmol) were added into the mixture solvent composed of 45 ml ethanol amine (EA) and 5 ml distilled water, which was then stirred to form a even solution. The above solution was transferred into Teflon-lined stainless steel autoclave, which was sealed and the contents warmed to 220 °C. After 24 h the contents was cooled to room temperature. The yellow-green products were collected by using a centrifuge, washed several times using distilled water and absolute ethanol, and dried under vacuum at 50 °C for 4 h.

The products were characterized by using X-ray diffraction (XRD) recorded on a Japanese Rigaku D/max-γA rotating anode diffractometer equipped with monochromatic high-intensity $Cu_{k\alpha}$ radiation ($\lambda=1.54178$). SEM images were taken with a FESEM (JEOL-6300F, 15 kV). Microscopy was performed by using a Hitachi (Tokyo, Japan) H-800 transmission electron microscope at an accelerating voltage of 200 kV, and a JEOL-2010 high-resolution TEM, also at 200 kV. XPS measurements were performed by using a VGESCA-LAB MKII X-ray photoelectron spectrometer with an excitation source of $Mg_{k\alpha}=1253.6$ eV. Raman spectra were recorded on a Jobin Yvon (France) LABRAM-HR confocal laser micro-Raman spectrometer at room temperature. UV/Vis spectra were recorded on a SolidSpec-3700 spectrophotometer at room temperature.

The photocatalytic measurements: The photocatalytic activity experiments on the obtained ZnSe nanobelts for the decomposition of fuchsine acid in air were performed at ambient temperature. Cylindrical Pyrex flasks (capacity ≈25 ml) were used as the photoreactor vessels. ZnSe nanoparticles as catalyst (10 mg) were added to the aqueous fuchsine acid solution ($C_{20}H_{17}N_3O_9S_3Na_2$) (Sigma-Aldrich, 1.0×10^{-4} M, 20 ml) and were magnetically stirred in the dark for 10 min to reach the adsorption equilibrium of fuchsine acid with the catalyst. The solutions were then exposed to UV light (high-pressure Hg lamp, 60 W). Commercial ZnSe and commercial TiO_2 powders (Degussa P25, Degussa, the surface area is $\approx45\ m^2g$) were adopted as references, to compare the photocatalytic activity under the same experimental conditions. UV/Vis absorption spectra were recorded at different intervals to monitor the reaction by using a SolidSpec-3700 UV/Vis spectrophotometer.

Acknowledgements

The financial support of this work, by the National Natural Science Foundation of China (No.20431020) and the 973 Project of China (No. 2005CB623601), is gratefully acknowledged.

[1] a) M. R. Hoffmann, S. T. Martin, W. Choi, D. W. Bahnemann, *Chem. Rev.* **1995**, *95*, 69; b) M. Anpo, M. Takeuchi, *J. Catal.* **2003**,

216, 505; c) J. S. Hu, L. L. Ren, Y. G. Guo, H. P. Liang, A. M. Cao, L. J. Wan, C. L. Bai, *Angew. Chem.* **2005**, *117*, 1295; *Angew. Chem. Int. Ed.* **2005**, *44*, 1269.

[2] a) I. Salem, *Catal. Rev. Sci. Eng.* **2003**, *45*, 205; b) A. L. Linsebigler, G. Lu, J. T. Yates, Jr., *Chem. Rev.* **1995**, *95*, 735.

[3] a) S. Yanagida, K. Mizumoto, C. J. Pac, *J. Am. Chem. Soc.* **1986**, *108*, 647; b) S. Yanagida, T. Azuma, Y. Midori, C. J. Pac, H. Sakurai, *J. Chem. Soc. Perkin Trans. 2* **1985**, 1487; c) W. F. Shangguan, A. Yoshida, *J. Phys. Chem. B* **2002**, *106*, 12227; d) G. Q. Guan, T. Kida, K. Kusakabe, K. Kimura, X. M. Fang, T. L. Ma, E. Abe, A. Yoshida, *Chem. Phys. Lett.* **2004**, *385*, 319; e) W. T. Yao, S. H. Yu, S. Liu, J. Chen, X. M. Liu, F. Q. Li, *J. Phys. Chem. A* **2006**, *110*, 11704; f) S. L. Xiong, B. J. Xi, C. M. Wang, D. C. Xu, X. M. Feng, Z. C. Zhu, Y. T. Qian, *Adv. Funct. Mater.* **2007**, in press.

[4] Z. M. Zhu, N. Z. Liu, G. H. Li, H. X. Han, Z. P. Wang, S. Z. Wang, L. He, R. B. Ji, Y. Wu, *Hongwai Yu Haomibo Xuebao (J. Infrared Millimeter Waves)* **1999**, *18*, 13.

[5] S. Z. Wang, S. F. Yoon, L. He, X. C. Shen, *J. Appl. Phys.* **2001**, *90*, 2314.

[6] a) Y. Jiang, X. M. Meng, W. C. Yiu, J. Liu, J. X. Ding, C. S. Lee, S. T. Lee, *J. Phys. Chem. B* **2004**, *108*, 2787; b) Q. Li, X. G. Gong, C. R. Wang, J. Wang, K. M. Ip, S. Hark, *Adv. Mater.* **2004**, *16*, 1436; c) X. T. Zhang, Z. Liu, K. M. Ip, Y. P. Leung, Q. Li, S. K. Hark, *J. Appl. Phys.* **2004**, *95*, 5752; d) Y. C. Zhu, Y. Bando, *Chem. Phys. Lett.* **2003**, *377*, 367; e) X. F. Duan, C. M. Lieber, *Adv. Mater.* **2000**, *12*, 298; f) R. Solanki, J. Huo, J. L. Freeouf, *Appl. Phys. Lett.* **2002**, *81*, 3864; g) J. Q. Hu, Y. Bando, J. H. Zhan, Z. W. Liu, D. Golberg, S. P. Ringer, *Adv. Mater.* **2005**, *17*, 975; h) J. Q. Hu, Y. Bando, D. Golberg, *Small* **2005**, *1*, 95; i) Q. Peng, Y. J. Dong, Y. D. Li, *Angew. Chem.* **2003**, *115*, 3135; *Angew. Chem. Int. Ed.* **2003**, *42*, 3027; j) W. Yao, S. H. Yu, J. Jiang, L. Zhang, *Chem. Eur. J.* **2006**, *12*, 2066; k) S. L. Xiong, J. M. Shen, Q. Xie, Y. Q. Gao, Q. Tang, Y. T. Qian, *Adv. Funct. Mater.* **2005**, *15*, 1787.

[7] a) M. Futsuhara, K. Yoshioka, O. Takai, *Thin Solid Films* **1998**, *322*, 274; b) G. Silversmit, D. Depla, H. Poelman, G. B. Marin, R. D. Gryse, *J. Electron Spectrosc. Relat. Phenom.* **2004**, *135*, 167.

[8] D. Sarigiannis, J. D. Peck, G. Kioseoglou, A. Petrou, T. Mountziaris, *Appl. Phys. Lett.* **2002**, *80*, 4024.

[9] B. Schreder, A. Materny, W. Kiefer, G. Bacher, A. Forchel, G. Landwehr, *J. Raman Spectrosc.* **2000**, *31*, 959.

[10] G. Lermann, T. Bischof, A. Materny, W. Kiefer, T. Kummell, G. Bacher, A. Forchel, G. Landwehr, *J. Appl. Phys.* **1997**, *81*, 1446.

[11] T. J. Mountaiaris, J. D. Peck, S. Stoltz, W. Y. Yu, A. Petrou, P. G. Mattocks, *Appl. Phys. Lett.* **1996**, *68*, 2270.

[12] M. B. Sigman, A. Ghezelbash, T. Hanrath, A. E. Saunders, F. Lee, B. A. Korgel, *J. Am. Chem. Soc.* **2003**, *125*, 16050.

[13] a) X. G. Peng, L. Manna, W. D. Yang, J. Wickham, E. Scher, A. Kadavanich, A. P. Alivisatos, *Nature* **2000**, *404*, 59; b) N. Cordente, M. Respaud, F. Senocq, M. J. Casanove, C. Amiens, B. Chaudret, *Nano Lett.* **2001**, *1*, 565; c) Y. W. Jun, S. M. Lee, N. J. Kang, J. Cheon, *J. Am. Chem. Soc.* **2001**, *123*, 5150.

[14] a) C. J. Johnson, E. Dujardin, S. A. Davis, C. J. Murphy, S. Mann, *J. Mater. Chem.* **2002**, *12*, 1765; b) S. H. Yu, H. Cölfen, K. Tauer, M. Antonietti, *Nat. Mater.* **2004**, *3*, 51; c) L. Wang, X. Chen, J. Zhan, X. Sui, J. Xhao, Z. Sun, *Chem. Lett.* **2004**, 720; d) C. J. Murphy, *Science* **2002**, *298*, 2139.

[15] a) E. Bae, W. Choi, *Environ. Sci. Technol.* **2003**, *37*, 147; b) J .J. He, A. Hagfeldt, S. E. Lindquist, *Langmuir* **2001**, *17*, 2743.

Received: February 28, 2007
Published online: July 6, 2007

